UNIVERSITY OF CALIFORNIA

Los Angeles

Circulation and Soil Moisture Contributions to United States Heatwaves

A thesis submitted in partial satisfaction

of the requirements for the degree Master of Science

in Environment and Sustainability

by

Russell Horowitz

2021

© Copyright by

Russell Horowitz

2021

ABSTRACT OF THE THESIS

Circulation and Soil Moisture Contributions

to United States Heatwaves

by

Russell Horowitz

Master of Science in Environment and Sustainability

University of California, Los Angeles, 2021

Professor Karen A. McKinnon, Chair

Extreme heat events are a threat to human health, productivity and food supply, so understanding their drivers is critical to adaptation and resilience. Anticyclonic circulation and certain quasi-stationary Rossby wave patterns are well-known to coincide with heatwaves, and soil moisture deficits amplify extreme heat in some regions. However, the relative roles of these two factors in causing heatwaves is still unclear. Here we use constructed circulation analogs to estimate the contribution of atmospheric circulation to United States heatwaves in the Community Earth System Model version 1 (CESM1) preindustrial control simulations. After accounting for the component of the heatwaves explained by circulation, we explore the relationship between the residual temperature anomalies and soil moisture. We find that circulation explains over 85% of heatwave temperature anomalies in the eastern and western US,

but only 70-80% in the central US. In this region, there is a significant negative correlation between soil moisture the week before the heatwave and the strength of the heatwave that explains additional variance. Further, for the hottest central US heatwaves, positive temperature anomalies and negative soil moisture anomalies are evident over a month before heatwave onset. These results provide evidence that positive land-atmosphere feedbacks may be amplifying heatwaves in the central US and demonstrate the geographic heterogeneity in the relative importance of the land and atmosphere for heatwave development. Analysis of future circulation and soil moisture in the CESM1 Large Ensemble indicates that over parts of the US, both may be trending towards greater heatwave likelihood.

The thesis of Russell Horowitz is approved.

Alan Barreca

Rong Fu

Karen A. McKinnon, Committee Chair

University of California, Los Angeles

2021

TABLE OF CONTENTS

LIST OF FIGURES

Supplementary Figures

ACKNOWLEDGMENTS

This thesis is a version of Horowitz, R.L., Simpson, I.R., and McKinnon, K.A. Circulation and Soil Moisture Contributions to United States Heatwaves. Submitted to *Journal of Climate*. Both Karen McKinnon and Isla Simpson were critical in guiding the research and analysis presented here, as well as editing this work.

I would like to acknowledge the generous financial support I received from NRT-INFEWS: Integrated Urban Solutions for Food, Energy, and Water Management (Grant DGE-1735325). As well, I acknowledge the CESM1 Large Ensemble Community Project, the computing resources provided by NCAR's Computational and Information Systems Lab, and National Science Foundation (Grant AGS-1939988).

1. Introduction

Extreme heat events are a threat to human health and quality of life. Positive temperature extremes increase human mortality and morbidity (Ye et al. 2012; Honda et al. 2014; Romero-Lankao et al. 2014; Gasparrini et al. 2015; Song et al. 2017) and decrease workplace and school productivity (Kjellstrom et al. 2009; Heal and Park 2016; Goodman et al. 2018). Further, our food supply can be damaged by crop exposure to extreme heat (Schlenker and Roberts 2009; Sánchez et al. 2014; Vogel et al. 2019).

Unfortunately, extreme heat is expected to occur more and more frequently as global temperatures increase. For example, between 1986 and 2016, more than twice as many high-temperature records were set in the United States as low-temperature records (Vose et al. 2017). It is therefore increasingly important to understand the physical drivers underlying these dangerous events. Improved prediction and modeling of the underlying factors and the resulting heatwaves may allow for better adaptation to lessen their negative impact on society.

Links between large-scale atmospheric circulation and summer heat extremes are well-established. Heatwaves are strongly associated with anticyclonic circulation that leads to subsidence and clear skies that support drying and warming of air (Meehl and Tebaldi 2004; Gershunov et al. 2009; Pfahl and Wernli 2012; Grotjahn et al. 2016; Adams et al. 2021). In some cases, these anticyclones are associated with quasi-stationary Rossby waves, which have been shown to cause extreme and long-lasting heat events (Schubert et al. 2011; Screen and Simmonds 2014; Röthlisberger et al. 2019), at times inducing co-occurring extremes around the mid-latitudes (Coumou et al. 2014; Kornhuber et al. 2019). Heat extremes can also be caused by horizontal advection of warm air (Lau and Nath 2012; Loikith and Broccoli 2012; Horton et al.

2016; Thomas et al. 2020), where the relevant source of the warm air depends on the location of the heat wave. For example, Yang et al. (2019) found associations with terrestrial warm air advection in the northern US and with oceanic warm air advection in the southern US.

In addition to the influence of large-scale circulation patterns, summer temperature extremes can be amplified or damped due to interactions with the land surface. In particular, soil moisture has been identified as an important mediator of interactions between the land surface and the atmosphere (Seneviratne et al. 2010, 2013; Grotjahn et al. 2016; Horton et al. 2016; Lo et al. 2017). Reductions in soil moisture can shift the partitioning of incoming heat from latent to sensible heating, thereby increasing the surface and lower atmospheric temperature (Fischer et al. 2007b; Miralles et al. 2014). The reduction in evapotranspiration can further increase temperatures by causing reduced cloud cover and decreased precipitation (Miralles et al. 2019; Selten et al. 2020).

Soil moisture deficits have been linked to specific extreme heat events in the United States and Europe (Fischer et al. 2007a; Hauser et al. 2016; Wehrli et al. 2019), and multiple studies have performed simulations with and without interactive soil moisture to show that land-atmosphere interactions amplify heatwaves (Lorenz et al. 2010; Jaeger and Seneviratne 2011; Stéfanon et al. 2014; Vogel et al. 2017). Focusing on the atmospheric response, Merrifield et al. (2019) performed a modeling experiment constraining circulation at different levels to demonstrate that heatwaves are intensified by land surface-atmosphere interactions. While these studies have quantified the influence of soil moisture in idealized settings and/or for individual events, we are lacking a more general diagnostic analysis of the relative roles of the atmosphere and the land surface in causing extreme heat.

Understanding the relative importance of soil moisture in heatwave development is especially worthwhile because of its potential predictive capacity. Soil moisture provides a memory of previous land-atmosphere conditions (Koster and Suarez 2001; Seneviratne et al. 2006), whereas the atmosphere is inherently chaotic and difficult to predict beyond short timescales. Antecedent precipitation, through its effect on soil moisture, has been identified as a predictor of heatwaves in some regions (Hirschi et al. 2011; Mueller and Seneviratne 2012; McKinnon et al. 2016). Therefore, quantifying the role soil moisture plays in extreme heat events across broad geographies may enhance our ability to predict heatwaves in the future.

Here, we take a unified approach to exploring the contribution of atmospheric circulation versus other processes to heatwaves in nine climate regions of the continental United States. We estimate the contribution of circulation to temperature anomalies by dynamically adjusting using constructed circulation analogs (Deser et al. 2016), which have been applied successfully to monthly temperatures during winter (Deser et al. 2016; Lehner et al. 2017) and summer (Merrifield et al. 2017). We apply this technique to control simulations in version 1 of the Community Earth System Model (CESM1; Hurrell et al. 2013) on a daily timescale, which allows us to quantify the impact of circulation on extreme heat events. We can then identify regions where there is substantial amplification of temperatures during heatwaves that is unexplained by the circulation and explore the importance of soil moisture for this amplification. Finally, we examine projected changes in the identified heatwave components – atmospheric circulation and soil moisture - in the CESM1 Large Ensemble (Kay et al. 2015).

The rest of this study is presented as follows. Section 2 describes the CESM1 datasets used and summarizes the constructed circulation analog technique, along with the modifications

we made to apply it to daily data. Section 3 shows the results of the dynamical adjustment and identifies future trends. The results and implications are discussed in Section 4.

2. Data and Methods

a. The CESM1 Control Simulations and Large Ensemble

We use data from simulations conducted with version 1 of the Community Earth System Model (CESM1) at 1° horizontal resolution with the full carbon cycle enabled. Two preindustrial control simulations are used, both with forcings representative of the year 1850. The primary dataset analyzed is a 1,799-year fully-coupled preindustrial control run (PiCTL). This is compared with a 2,600-year preindustrial control run, of which only the first 1,799 years are used, where sea surface temperatures are prescribed to those of the seasonally varying monthly climatology from PiCTL (fixSST-PiCTL).

Future projections are from the CESM1 Large Ensemble (CESM1-LE; Kay et al. 2015). This consists of 40 ensemble members that have the same radiative forcing, but slightly perturbed initial atmospheric conditions, allowing internal variability to lead to a range of possible outcomes (Deser et al. 2016). The ensemble members differ only in a very small round-off error to the initial air temperature on January 1, 1920. These runs are forced by historical radiative forcing from 1920 to 2005, then by RCP 8.5 radiative forcing until 2100 (Taylor et al. 2012).

We use daily average 2m air temperature (hereafter simply temperature), sea level pressure, surface latent heat flux, surface sensible heat flux, 500 hPa geopotential height, and soil moisture in the top 10cm of soil for our analysis. The climatological mean and seasonal cycle of

each variable at each grid box is removed by projecting the time series onto the first three annual harmonics, then subtracting the fitted values. All of our analysis focuses on the summer season, June-July-August (JJA), in the continental US. We split the continental US into the 9 climate regions identified by Karl and Koss (1984). These climate regions are identified in Figure 1a. While each region is analyzed separately, some figures presented in this paper will combine the results from all regions into a single map.

b. Constructed Circulation Analogs for Daily Temperature

To calculate the daily dynamical component of the temperature distribution in each region, we implement constructed circulation analogs (CCAs; Deser et al. 2016). A brief summary of the CCA method, with modifications made for this study, follows. To estimate the dynamical contribution to temperature anomalies for a target day in a given region, we begin with the sea level pressure (SLP) from the target day. The SLP pattern comes from a larger spatial domain than the actual climate region whose temperature is of interest. We automatically selected an area that extends 54° west, 18° east, 15° north and 15° south of the center of the region. This domain is chosen to span the wavelength of a wavenumber-5 pattern, since patterns with wavenumber-5 are often associated with summer temperature extremes in North America (Teng et al. 2013; Screen and Simmonds 2014; Kornhuber et al. 2020). An example of this broader SLP region relative to the specific region of interest is shown in Figure 1b.

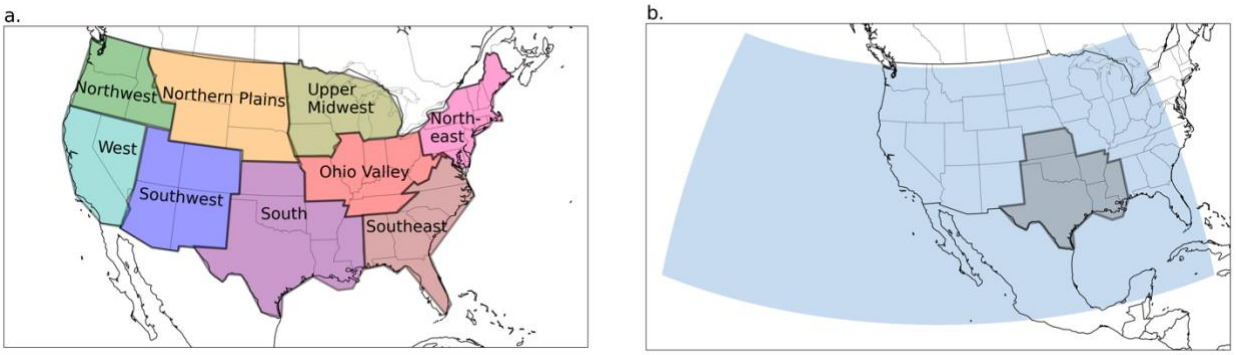

Figure 1. Climate regions. a) The nine climate regions used in this analysis (Karl and Koss, 1984) and (b) the South region, in gray, and its broader sea level pressure region, in blue, used for the constructed circulation analogs.

Closely matching SLP analogs are found from other days in the simulation. The SLP analogs may come from N_y years in the same preindustrial control simulation, which cannot include the same year as the target day. The maximum value for N_y is therefore 1,798 years, one year less than the total length of the control simulation, and we explore the effect of decreasing N_y below. To account for the differing seasonal effects of circulation on temperature, only days between one week before and one week after the day of summer being analyzed are allowed as potential analogs. The importance of this constraint is shown in Figure 2. Although we have removed the seasonal cycle in SLP and temperature, the temporal standard deviation of SLP, averaged across the broader wave 5 domain, and temperature, averaged across the regions of interest, are not stationary throughout the summer. The standard deviation of SLP decreases in June and July and increases in August in all regions and both increasing and decreasing trends across the summer are present for temperature standard deviation. It is therefore reasonable to expect that the same SLP pattern in June and August may produce different temperature responses, which will be limited by placing the two-week restriction on analogs. This restriction means that for any given day, there are 15 days from each of the N_y years that can potentially be used as

analogs, but no more than one day per year is selected to eliminate the risk of selecting multiple analogs from the same circulation event.

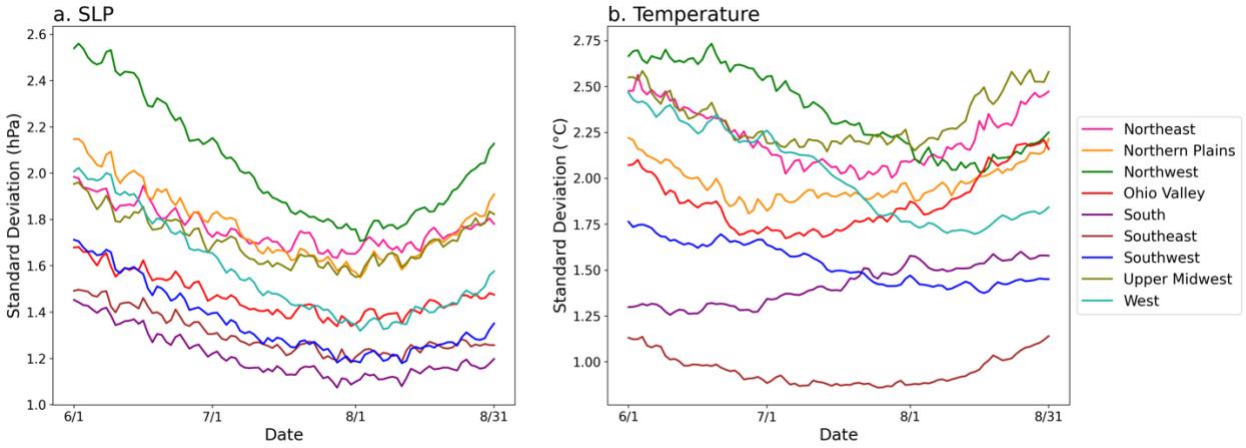

Figure 2. SLP and temperature standard deviation. The area-weighted standard deviation of (a) mean sea level pressure anomaly and (b) mean temperature anomaly across all years of the fully-coupled preindustrial control simulation for each date of the summer. The mean sea level pressure is taken over the entire spatial domain used in the constructed circulation analogs, while the mean temperature is taken over only the region of interest.

After specifying the pool of potential analogs, we identify the N_a closest options as measured by the lowest Euclidean distance to the target SLP pattern. Given a set of analogs, ordinary least squares regression is performed to obtain the weights of the analogs to match the target SLP field. The weights from this regression are then applied to the temperature anomalies from the analogs to estimate the dynamical contribution to the target day's temperature anomalies at each grid cell in the region. In order to reduce the noise in our method, we subsample N_s analogs from our set of N_a options without replacement to generate the dynamical component. This is repeated N_r times, with the final dynamical component estimated as the mean estimated dynamical component of all N_r samples following Deser et al. (2016). We vary both the number of repeated samples and the number of analog years to assess the sensitivity of the results to these values (Section

3a). For our primary analysis, we use the same values as Deser et al. (2016) for $N_a = 150$ and $N_s = 100$, as well as $N_r = 20$ and the maximal value of $N_y = 1{,}798$.

3. Results

a. Daily CCA Performance

Although the focus of this paper is on heat extremes, we are also interested in the performance of dynamical adjustment on daily timescales, as most previous work has focused on monthly or seasonal temperature averages. Deser et al. (2016) showed that when using CCAs for winter temperature over North America, the average root mean squared error (RMSE) converged with N_r less than 20. Here, we vary N_y, the number of analog years, and N_r, the number of subsamples averaged over each analog selection. Then we calculate the average RMSE for temperature for each region and over the entire continental US for summer. The sensitivity of RMSE to N_r, in Figure 3a, is very similar to that found by Deser et al. (2016). The thick black line indicates the RMSE over the entire continental United States, while the colored lines show the results for all regions. Increasing N_r, while keeping N_y constant at its maximum value of 1,798, results in average summer RMSE declining approximately exponentially, but plateauing before $N_r = 20$, which is the value used in this analysis. All regions follow a very similar pattern of exponential decline. The main difference between regions is the value they plateau at. Regions with greater variability in summer temperature will tend to have greater RMSE values, as will regions where SLP is less related to temperature variation. Many of these regional differences in the performance of the CCAs hold when looking at heatwaves as well and will be discussed more below.

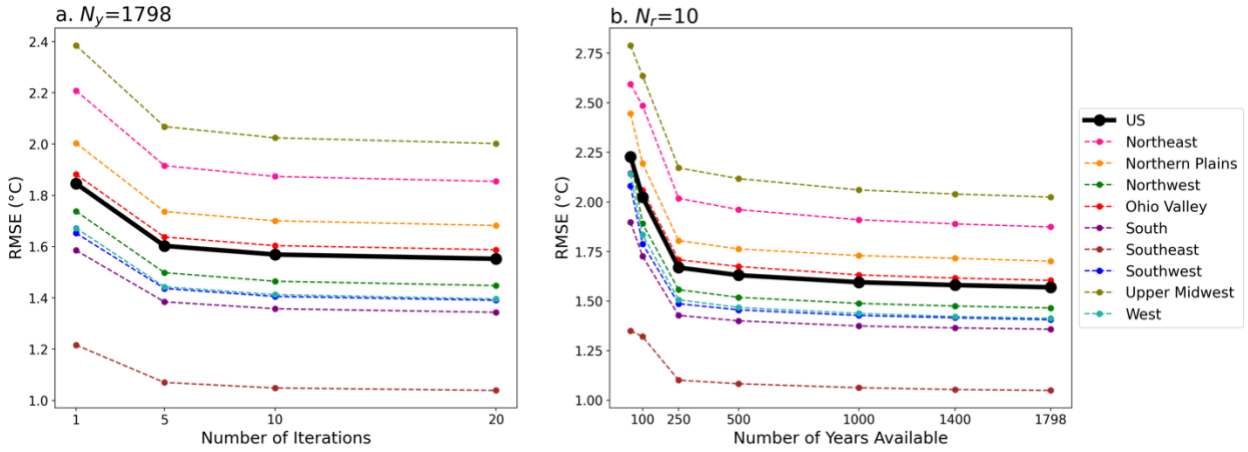

Figure 3. Temperature RMSE. The area-weighted root-mean-squared-error (RMSE) for summer temperature averaged in the continental US (black) and each climate region (colors) for the fully-coupled preindustrial control simulation. Constructed circulation analogs are performed with varying (a) N_r, with N_y set at 1,798, and (b) N_y, with N_r set at 10. N_r is the number of iterations of the constructed circulation analog procedure that is performed and averaged for each day. N_y is the number of years of analogs to select from.

Figure 3b shows the sensitivity of RMSE to the number of years of analogs, with N_r kept constant at 10. N_y is varied from 50 years to 1,798 years. The RMSE again appears to decrease exponentially, roughly converging after more than 500 years are available. This seems to indicate that results for this analysis would not be substantially different with a longer preindustrial control run. However, this has important implications for working with observations, where many fewer analogs are available. Daily CCAs may perform poorly if too few sufficiently close analogs exist.

b. Heatwave and CCA Results

Candidate heatwaves for each region are defined as the hottest consecutive seven-day period in each summer, averaged over all grid cells, area-weighted, in each region. Each of these heatwaves has an associated dynamical component that has been estimated from the CCAs. This dynamical component is interpreted as the expected contribution of atmospheric circulation to the heatwave. Since we are selecting weeks that are abnormally hot, the average dynamical component from all heatwaves will be greater than zero. However, this definition assumes that

there is a heatwave in every summer, so many weeks that fit this criterion are not particularly extreme. Therefore, only those heatwaves with an estimated dynamical component in the 85th percentile or greater are analyzed, leaving us with 270 heatwaves per region across the full control simulation. It is these events that we will refer to as heatwaves in the remainder of this study. Filtering in this manner isolates events with a circulation pattern that is expected to be associated with extreme heat, and the circulation patterns for the events in each region are very similar.

The residual component of the temperature anomaly during each heatwave, calculated as the actual temperature anomaly minus the dynamical component, is unexplained by the linear relationship with concurrent SLP that is captured with the CCA methodology. Any influence of land-surface preconditioning, the prior time evolution of the circulation leading up to the heatwave, and/or nonlinear circulation-temperature relationships will be present in this residual. Our aim is to dissect the residual to explore the influence of land-atmosphere coupling during events with a similarly extreme expected dynamical contribution.

Mean temperature anomalies in PiCTL during these extreme events are displayed in Figure 4a. Temperature anomalies are highest in the Northwest, reaching up to 6.51°C with a regional average anomaly of 4.45°C. The West and most of the northern regions (Northern Plains, Upper Midwest, Ohio Valley, and Northeast) have more moderate extreme heat weeks, with regional averages ranging between 3.07°C and 4.01°C, while the southern regions (Southeast, South, Southwest), have smaller anomalies, between 1.55°C and 3.03°C. Figure 4b displays the intra-seasonal standard deviation of temperature during the summer in PiCTL, calculated as the square root of the average variance of daily temperatures during each summer.

The pattern of heatwave magnitude in Figure 4a generally follows this spatial pattern in summer temperature standard deviation, but with some important differences. Both heatwave magnitude and standard deviation tend to increase from south to north, with the greatest values in the Northwest and the smallest values in the Southeast. However, the South region and Northern Plains region, particularly over Oklahoma, North Dakota, and South Dakota, stand out as areas where the average heatwave magnitude is greater than one might expect from the summer temperature standard deviation.

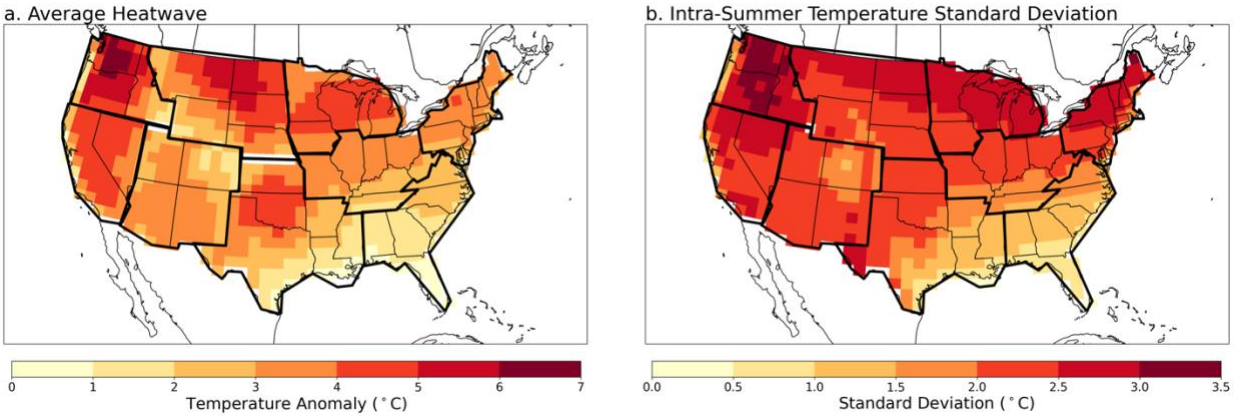

Figure 4. Temperature anomalies and standard deviations. In the fully-coupled preindustrial control simulation, (a) Average temperature anomaly during heatwaves and (b) daily summer temperature standard deviation, calculated as the square root of the average of the variances calculated for each summer individually

The temperature anomalies associated with the heatwaves are qualitatively similar in the fixSST-PiCTL control simulation (Figure S1), indicating the dominance of atmospheric and land processes in controlling the statistics of the heatwaves. Three regions, the Southwest, Upper Midwest, and Northern Plains show a slightly larger anomaly in PiCTL than fixSST-PiCTL by between 0.14°C and 0.18°C, while differences for all other regions are below 0.07°C. Given the overall small differences between PiCTL and fixSST-PiCTL, we primarily present results using only the fully-coupled control simulation.

While some regions have spatial homogeneity in the average temperature anomaly during heatwaves, a number of regions have spatial variation that could affect results when analyzing the region as one unit or be indicative of poor regional grouping. In particular, the South region is more extreme in its northern portion, and the eastern Northwest/western Northern Plains are less extreme than the rest of those regions. It is possible that we see these differences because certain parts of a region do in fact experience less-extreme temperatures during heatwaves or that the region experiences spatially asynchronous heatwaves. Since a heatwave is defined as the hottest summer week over the entirety of a region, a single event could occur more strongly in one part of the region than another. This effect is likely removed by averaging over many events, but it is possible that there is a weak association in heatwave temporal occurrence, with one part of the region dominating the most extreme weeks. While not pursued here, an alternative approach to using pre-specified climate regions is to use clustering methods to objectively identify regions that experience extreme heat events at the same time (Lau and Nath 2012; McKinnon et al. 2016; Kornhuber et al. 2020).

The average SLP pattern associated with heatwaves for each region is shown in Figure 5. Regions in the western and central US tend to exhibit negative SLP anomalies during heatwaves, likely indicating the presence of thermal lows caused by elevated surface temperatures. Most regions exhibit a boundary between positive and negative SLP anomalies close to or inside of the region. This potentially indicates a role for advection during these events, depending on the orientation of the boundary. For example, the geostrophic flow associated with the Northwest SLP pattern, Figure 5c, is southerly, which would bring warm air from the interior west into the region. Likewise, in the Ohio Valley, Figure 5d, the geostrophic flow would bring warmer air

from the southwest. In contrast, for the Northern Plains, Figure 5b, the geostrophic flow is northerly and would therefore, on average, bring cooler air into the region.

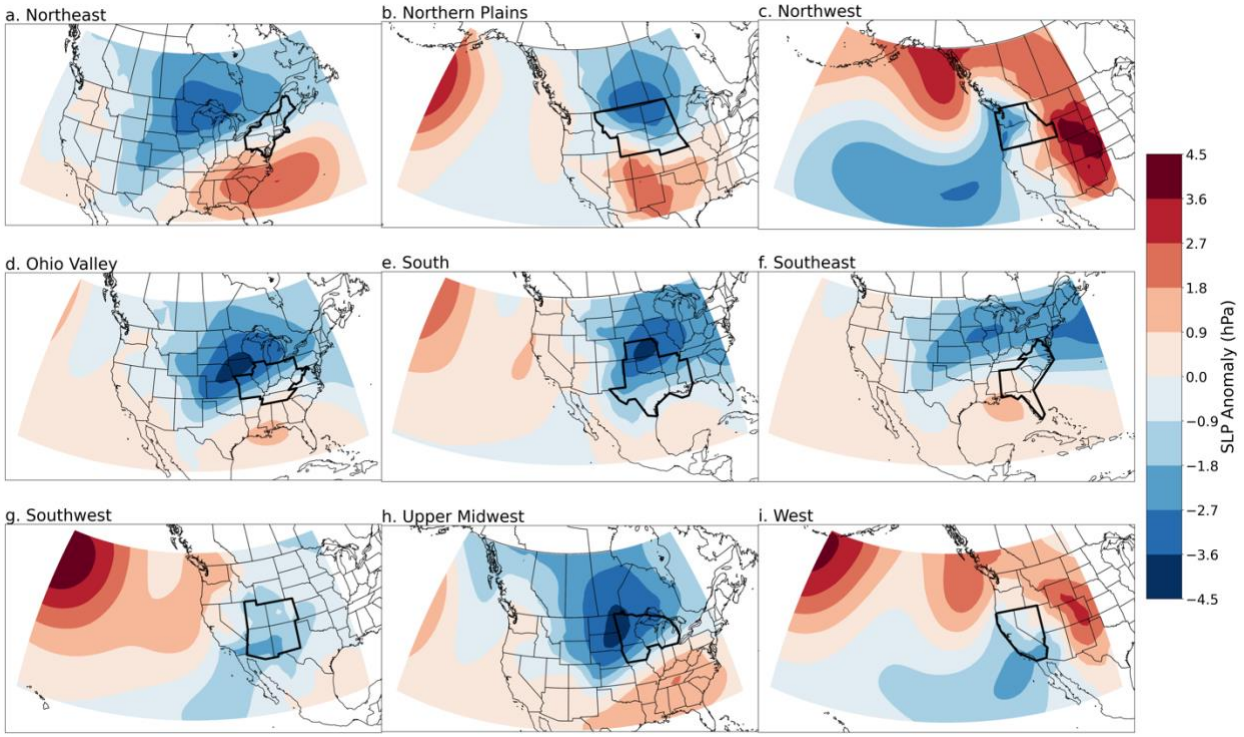

Figure 5. Heatwave SLP patterns. Average sea level pressure anomaly pattern during heatwaves in the fully-coupled preindustrial control simulation. The region of interest is outlined in black. The colored area shown is the spatial region used for sea level pressure in the constructed circulation analogs

To further understand the meteorology of these events, the average 500 hPa geopotential height anomalies (Z500) are shown in Figure 6. The Z500 anomalies are more consistent across regions than SLP, with all regions containing or near the center of a Z500 high, although the magnitudes of the geopotential height anomalies vary substantially. These high-pressure patterns likely are both a cause of and a response to the extreme heat. For the former, high atmospheric pressure is associated with clear skies and enhanced solar radiation at the surface; for the latter, Z500 will increase as the atmospheric column warms. While Merrifield et al. (2017) found that Z500 performed better as an explanatory variable than SLP in some regions in the US, we

choose to use SLP as our atmospheric circulation proxy to be consistent with the majority of the CCA literature (Deser et al. 2016; Lehner et al. 2017, 2018).

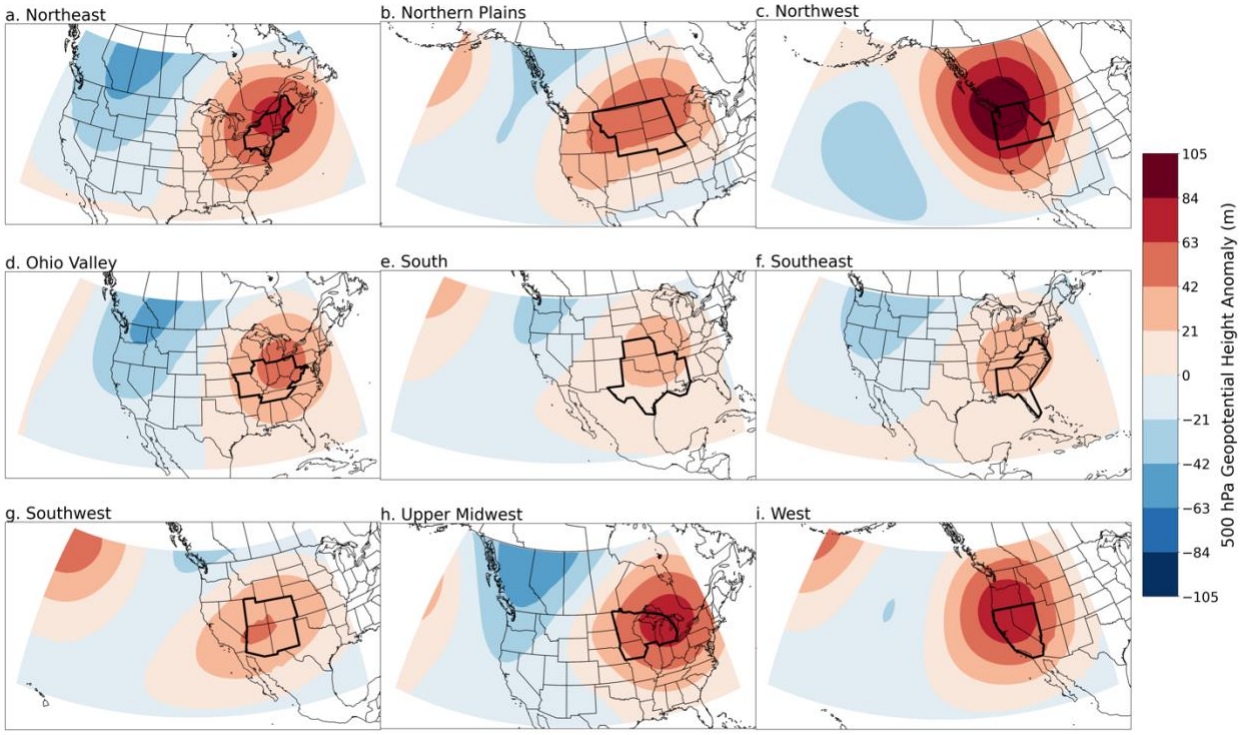

Figure 6. Heatwave Z500 patterns. Average geopotential height anomaly at 500 hPa during heatwaves in the fully-coupled preindustrial control simulation. The region of interest is outlined in black. The colored area shown is the spatial region used for sea level pressure in the constructed circulation analogs.

The average component of the temperature anomaly unexplained by the dynamical prediction from the CCAs for these extreme events is shown in Figure 7a, and the proportion of the anomaly that is unexplained is displayed in Figure 7b. The dynamical component accounts for over 85% of the temperature anomalies along the western coast of the United States. Throughout most of the rest of the United States, the dynamical component accounts for at least 80% of heatwave temperature anomalies. The main exception is in the central US, spanning the South and Northern Plains climate regions, where greater than 20% of heatwave anomalies are unexplained. This is also true for the Southeast, in Florida and along the Atlantic coast, but since heatwave anomalies are relatively small here (see Figure 4a), the magnitude of the residual

temperature anomaly is also quite small compared to other regions. The central US stands out as having a larger residual component measured in both temperature anomaly and proportion.

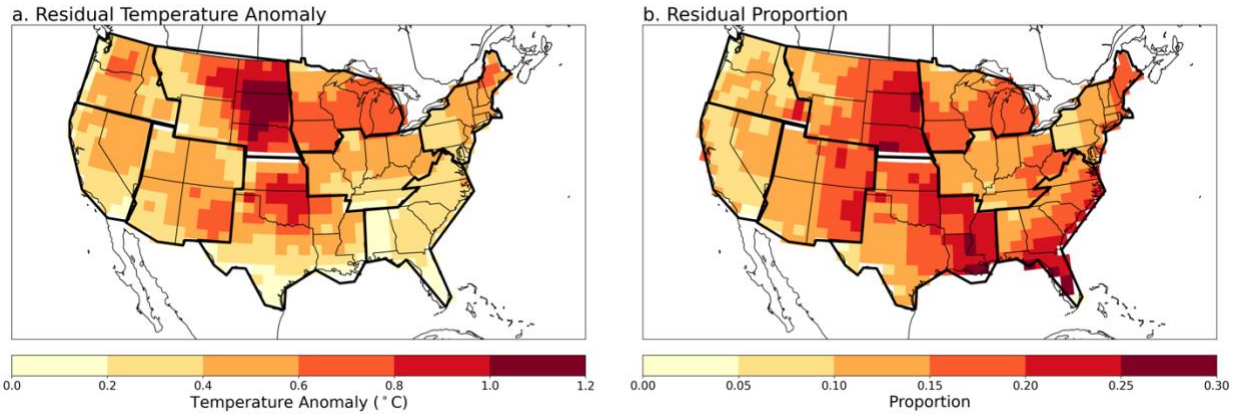

Figure 7. Residual temperature anomaly and proportion. For heatwaves in the fully-coupled preindustrial control simulation, (a) average residual temperature anomaly during heatwaves after removing the average dynamical component from the temperature anomaly and (b) proportion of the average heatwave temperature anomaly accounted for by residual temperature anomaly.

Even in the central US, the residual component never exceeds 30% of the heatwave anomaly on average. This indicates that, as expected, the largest explanatory factor for extreme heat is atmospheric circulation. Nevertheless, the residual component is important to understand for two regions. First, inasmuch as it is linked to boundary conditions, it may allow for predictability on longer-than-weather timescales (Hirschi et al. 2011; Mueller and Seneviratne 2012; McKinnon et al. 2016). Second, given the nonlinear nature of impacts of extreme heat (e.g. Anderson and Bell 2009; Schlenker and Roberts 2009), the amplification of temperature anomalies by 20-30%, as seen on average in the central US, is not inconsequential.

Despite the low proportion of heatwave temperature anomalies explained by the residual component across some of the United States, the average residual component in all grid cells is positive. Heatwaves have both a circulation pattern associated with positive temperature anomalies (a dynamical component greater than zero, by design) and are hotter than circulation alone would predict (a residual component greater than zero), indicating a likely role for positive

land surface feedbacks on the hottest weeks. This is consistent with prior work showing that the land surface tended to amplify, not damp, heat extremes (Lorenz et al. 2010; Jaeger and Seneviratne 2011; Stéfanon et al. 2014; Vogel et al. 2017).

c. The Role of Soil Moisture

Motivated by the body of research that identifies soil moisture as an important factor for temperature variability and extremes during summer (Seneviratne et al. 2010, 2013; Horton et al. 2016; Grotjahn et al. 2016; Lo et al. 2017), its impact on the residual component is explored below. The correlation between the residual component and the average soil moisture in the top 10cm of soil one week prior to each heatwave is displayed in Figure 8a. Only those correlations that are significant when controlling for a false discovery rate of 0.05 are colored (e.g. Wilks 2016). We examine the preceding, rather than synchronous, soil moisture because heatwaves can both be amplified by and cause low soil moisture; a deficit prior to the heatwave is suggestive that the heatwave-associated circulation pattern occurred over pre-conditioned dry soils. The residual component is significantly negatively correlated with one-week lagged soil moisture in a large swath of the central US, with smaller regions of negative correlations in Northern California and Oregon, and the Southeast. The region of large negative correlations in the central US roughly aligns with areas that have a larger residual proportion in Figure 7b. In particular, the South, Northern Plains, and western Ohio Valley have greater associations between their residual component and deficits in soil moisture, with average correlations of -0.40, -0.32, and -0.24 across the regions, respectively.

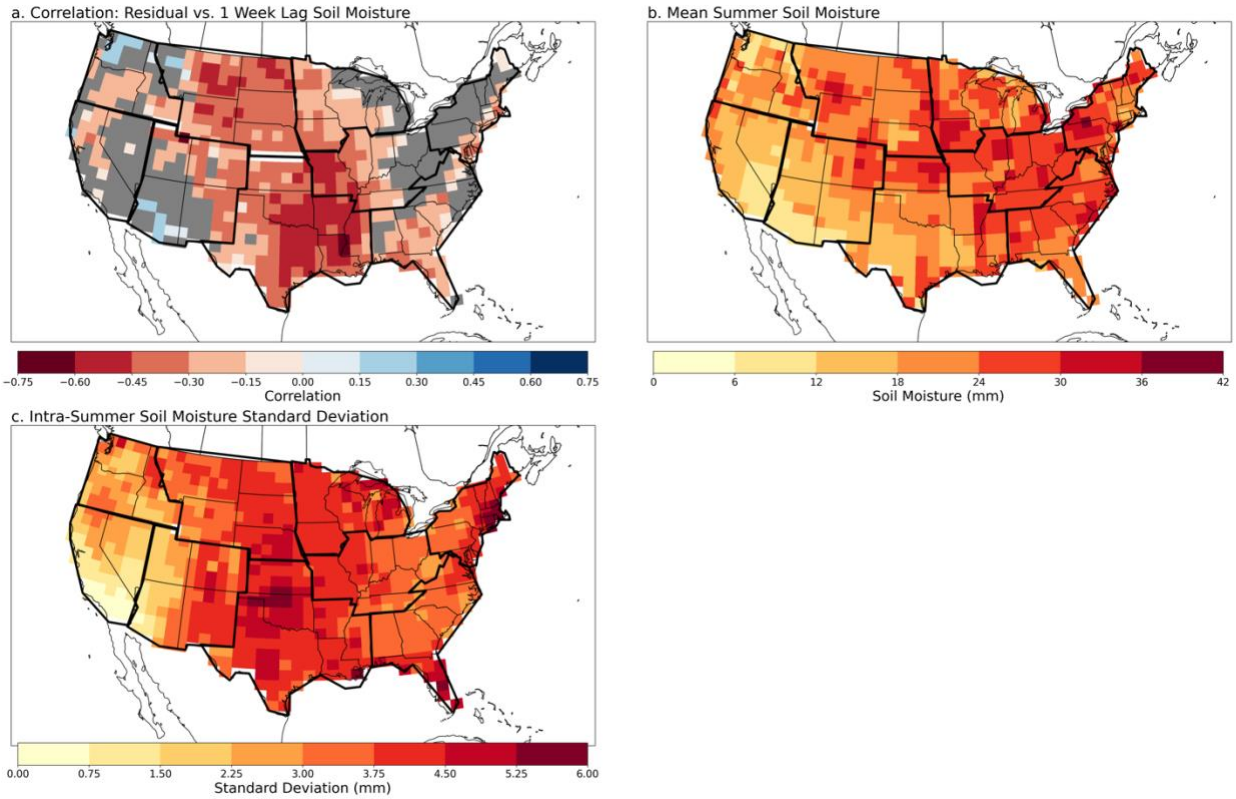

Figure 8. Soil moisture correlation, mean, and standard deviation. (a) Correlation between average residual temperature anomaly during a heatwave and average soil moisture anomaly the week before the heatwave for fully-coupled preindustrial control simulation heatwaves. Grid cells that are not significant when controlling for a false discovery rate of 0.05 are grey. (b) Mean summer soil moisture and (c) daily summer soil moisture standard deviation, calculated as the square root of the average of the variances calculated for each summer individually.

The spatial structure of the correlation map is related to the spatial structure in mean and variance of soil moisture. In the western US, both the mean soil moisture and its intra-seasonal standard deviation are small; in these dry regimes, soil moisture does not typically have an impact on temperature (Seneviratne et al. 2010). On the east coast, although soil moisture variability is greater, the correlation with the residual component is still near zero, consistent with the region being “energy limited”, as opposed to “moisture limited” (Teuling et al. 2009). Therefore, we expect variations that alter the radiation reaching the surface, such as cloudiness, to be more important. In contrast, the central US is a classic transitional region with low enough mean soil moisture to be moisture limited (Vargas-Zeppetello et al. 2020) and high soil moisture

variability, leading to greater potential for soil moisture variations to alter the surface energy balance and amplify the near-surface temperature.

The difference between moisture-limited and energy-limited regimes is further explored in Figure 9, which shows the average sensible and latent heat flux anomalies from 31 days prior to the start of a heatwave through the last day of the heatwave. The South climate region is selected to represent the moisture-limited case, whereas the Northwest and Northeast both represent energy-limited regimes. In the South, latent heat anomalies decrease as temperature rises during a heatwave, indicating a moisture limitation; in tandem, sensible heat flux anomalies at the surface increase, further increasing near-surface air temperature. The trends are in the opposite direction for the Northeast and Northwest, although with a lesser relative magnitude. In response to additional heating in these regions, additional water is evaporated or transpired from the land surface, leading to an increase in latent heat flux anomalies. The decrease in sensible heat fluxes indicates that the ground is cooler than the overlying atmosphere for these heatwaves (not shown), highlighting the importance of processes like advection over soil moisture-mediated heating. While we do not explore the role of humidity in heat waves here, the increase in latent heat in the energy-limited regimes will lead to increases in near-surface humidity, and therefore a higher heat index for a given temperature anomaly.

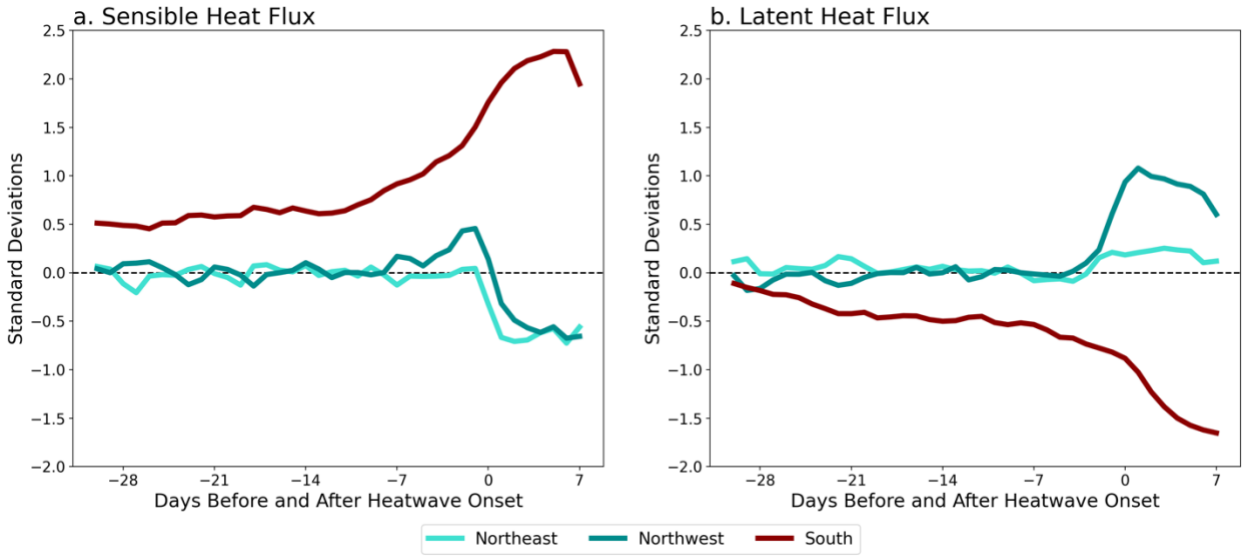

Figure 9. Sensible and latent heat flux progression. For heatwaves in the fully-coupled preindustrial control simulation in three representative regions, (a) average sensible heat flux anomalies, and (b) average latent heat flux anomalies for 31 days before the start of the heatwave (day 1) through the last day of the heatwave (day 7). The fluxes are measured in standard deviations, which have been calculated for each region as the square root of the area-weighted average of the variances calculated for each summer individually.

In order to see the differing relationship between soil moisture and heatwaves for moisture versus energy limited regimes, Figure 10 shows the progression of temperature anomalies, the estimated dynamical components (i.e. those temperature anomalies predicted by each day's SLP), and soil moisture anomalies for the South, Northeast, and Northwest from 31 days prior to the start of the heatwave through the end of the event. Heatwaves are split into the bottom and top quartile of residual component (the difference between the actual temperature anomaly and the dynamical component) magnitude and averaged. We would expect the higher residual events and the regions with stronger negative correlation between soil moisture and the residual component to demonstrate larger soil moisture deficits. This holds true, with the South experiencing larger soil moisture deficits during heatwaves than the Northwest and Northeast, as well as larger deficits in the high residual cases than low residual cases in all regions. However, Figure 10 also reveals a stark contrast in how long high residual events last compared to low

residual events in the moisture limited (South) versus energy limited (Northwest and Northeast) regions.

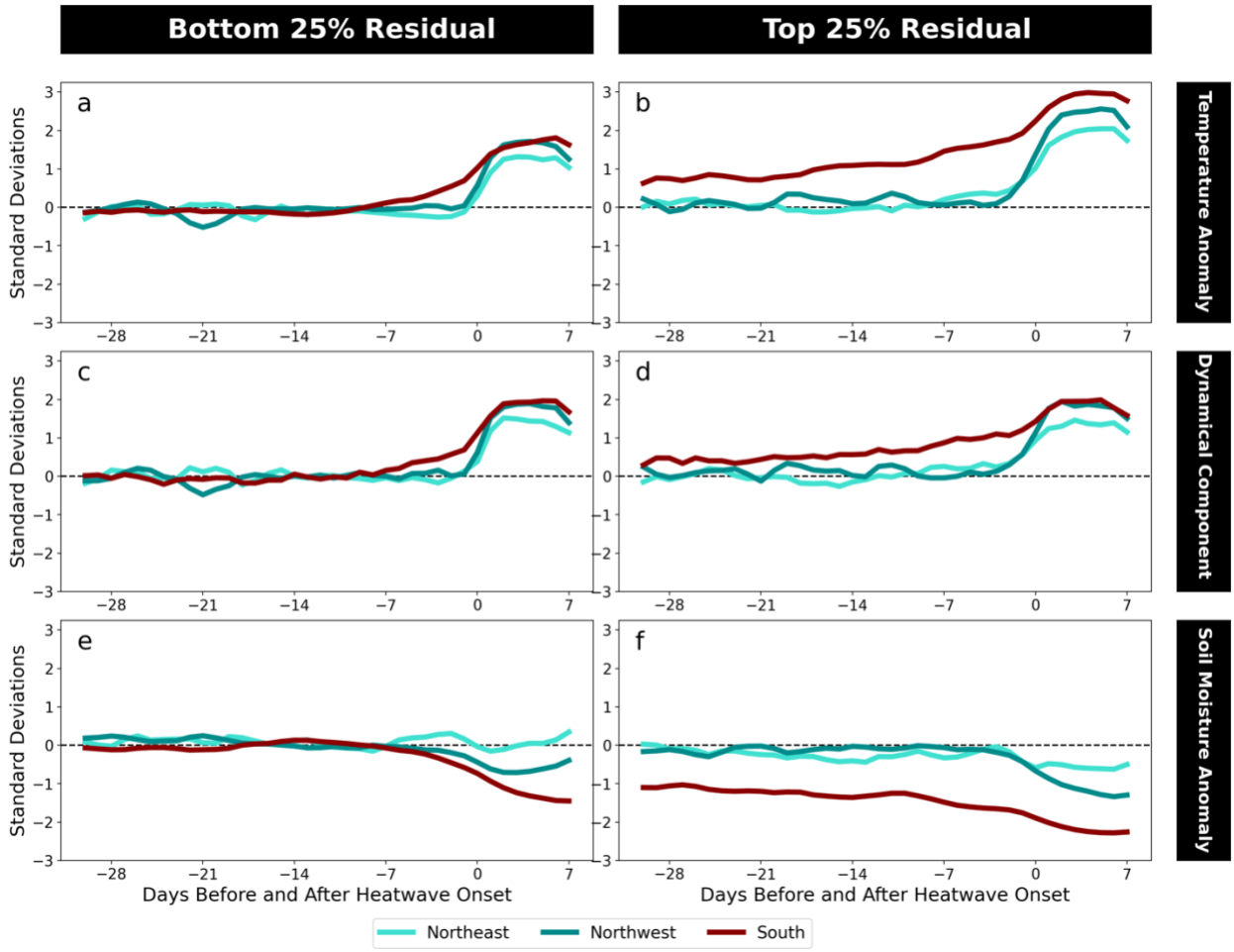

Figure 10. Temperature, dynamical component, and soil moisture progression. Heatwave progression in three representative regions for heatwaves with residual components in the lower quartile (a, c, e) and upper quartile (b, d, f) of fully-coupled preindustrial control simulation heatwaves. Displayed are (a) and (b) average temperature anomalies, (c) and (d) average dynamical component, and (e) and (f) average soil moisture anomalies for 31 days before the start of the heatwave (day 1) through the last day of the heatwave (day 7). The values are measured in standard deviations, which has been calculated for each region as the square root of the area-weighted average of the variances calculated for each summer individually. The dynamical component is measured in temperature standard deviation.

During low residual events, in which the temperature during the heatwave week can be better predicted using SLP analogs, all three regions behave similarly. Temperature anomalies begin increasing one to two days prior to the start of the heatwave week, rising rapidly as the extreme heat-associated circulation pattern occurs, and peaking near 1.5 standard deviations

above the climatological temperature. The behavior of the dynamical prediction is nearly identical, as expected. Significant soil moisture anomalies generally only occur during the heatwave week or a few days before, as the elevated temperature leads to increased evapotranspiration from the surface.

On the other hand, there is a marked difference between the regions during high residual events. The Northwest and Northeast behave largely the same as during low residual events, but with greater magnitudes in the size of anomalies during the heatwave week. These regions again experience elevated temperature anomalies a few days before the heatwave week, but now increase in temperature more rapidly, peaking closer to 2 standard deviations. The dynamical component also increases a few days before, but only peaks at 1.5 standard deviations (by definition, a high residual event will have a discrepancy between its temperature anomaly and its dynamical component). The soil moisture again declines only during the week of the heatwave. The decrease in soil moisture is greater, likely due to the higher temperatures inducing more evapotranspiration.

In the South, there is very different behavior in the high residual events compared to the low residual events. The peak heatwave temperature is 55% greater than the dynamically predicted temperature, in part due to the increased sensible heat fluxes linked to the low soil moisture. Positive temperature anomalies and negative soil moisture anomalies extend back for the full 31-day period prior to the heatwave. While the rate of change in temperature does peak at the start of the heatwave week, the heatwave is building upon a long period of hot and dry conditions. These persistent hot and dry conditions are not entirely explained by circulation, as the temperature anomaly exceeds the dynamical component throughout the period. This indicates

an important role for soil moisture preconditioning in the South: while we may not be able to predict a heatwave 31 days in advance, the presence of anomalously low soil moisture at that lead time would suggest that any future heatwave-associated circulation pattern will likely result in more extreme temperatures.

d. Future Trends

Having identified the circulation patterns and soil moisture anomalies associated with extreme heat, we next explore whether the probability of these heatwave ingredients is projected to change. To assess potential future changes, we use the CESM1-LE. Using all 40 ensemble members limits the impact of internal variability on the results, allowing a clearer picture of the forced response to human influence in the model.

Focusing first on projected forced circulation changes, we calculate the spatial correlation between each summer day in CESM1-LE and the average heatwave SLP pattern from PiCTL (the patterns seen in Figure 5). For each region, these correlations are calculated over the same expanded spatial domain that was used for the CCAs. The results, shown as the percentage of summer days per decade with a spatial correlation greater than 0.7, are plotted in Figure 11. Controlling for a false discovery rate of 0.05, there is a statistically significant positive trend over the period 2010-2099 in CESM1-LE in six of the nine regions and a statistically significant negative trend in the remaining three regions. For those regions with an increasing trend, the percentage is generally stable in the historical period, before increasing rapidly over the 21st century. In many of the regions, over twice as many days in 2090-2099 have a correlation greater than 0.7 compared to the historical period.

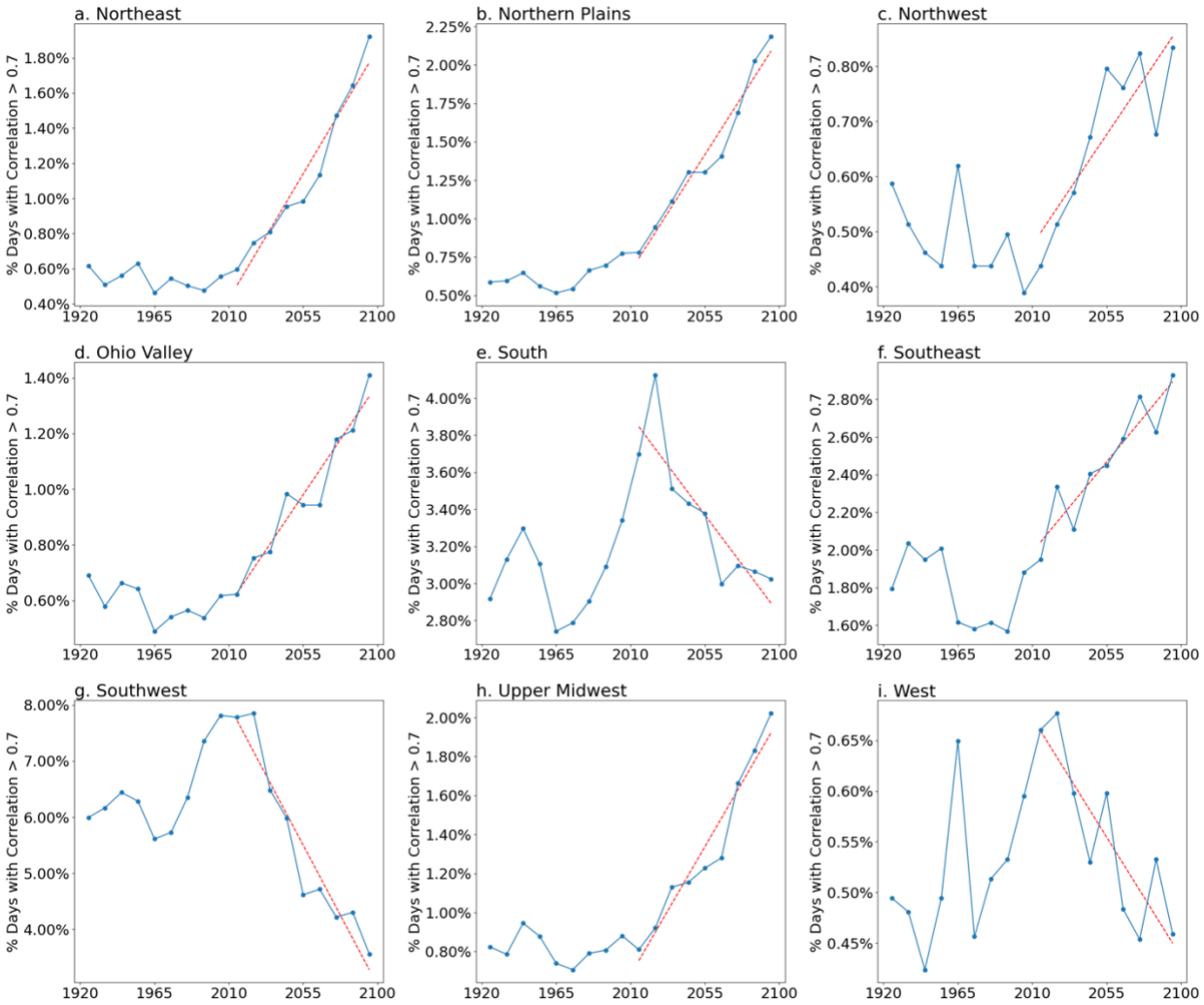

Figure 11. CESM1-LE SLP trends. By decade, percentage of days with a correlation above 0.7 between daily summer sea level pressure patterns in CESM1-LE and the average sea level pressure pattern for fully-coupled preindustrial control simulation heatwaves. Linear trend lines for 2010-2099 are shown in red.

To further understand these increases, we define a heatwave-associated event as one or more consecutive days with an SLP pattern that has a correlation greater than 0.7 with the PiCTL heatwave pattern. For the regions with an increasing percentage of days exhibiting heatwave-associated SLP patterns, we find that the increase is primarily driven by an increase in the number of separate events per year with the heatwave SLP patterns, although there are also small increases in event duration (Figures S3 and S4). This increasing trend in circulation events similar to those associated with heatwaves indicates a potential forced response in the dynamic

controls on extreme heat. However, given that heatwaves can also influence SLP, this analysis alone cannot conclusively establish causation.

Previous studies have identified decreasing trends in future projections of soil moisture in the American West (Mankin et al. 2017), Southwest (Seager et al. 2013; Cook et al. 2015) and Central Plains (Cook et al. 2015). Here we focus on trends in soil moisture in the South and Northern Plains regions of the US in the CESM1-LE, since these two regions displayed stronger links between the residual component of temperature and soil moisture anomalies. The trend in decadal average summer soil moisture for these two regions is displayed in Figure 12. The values are measured in each region's intra-summer PiCTL soil moisture standard deviation.

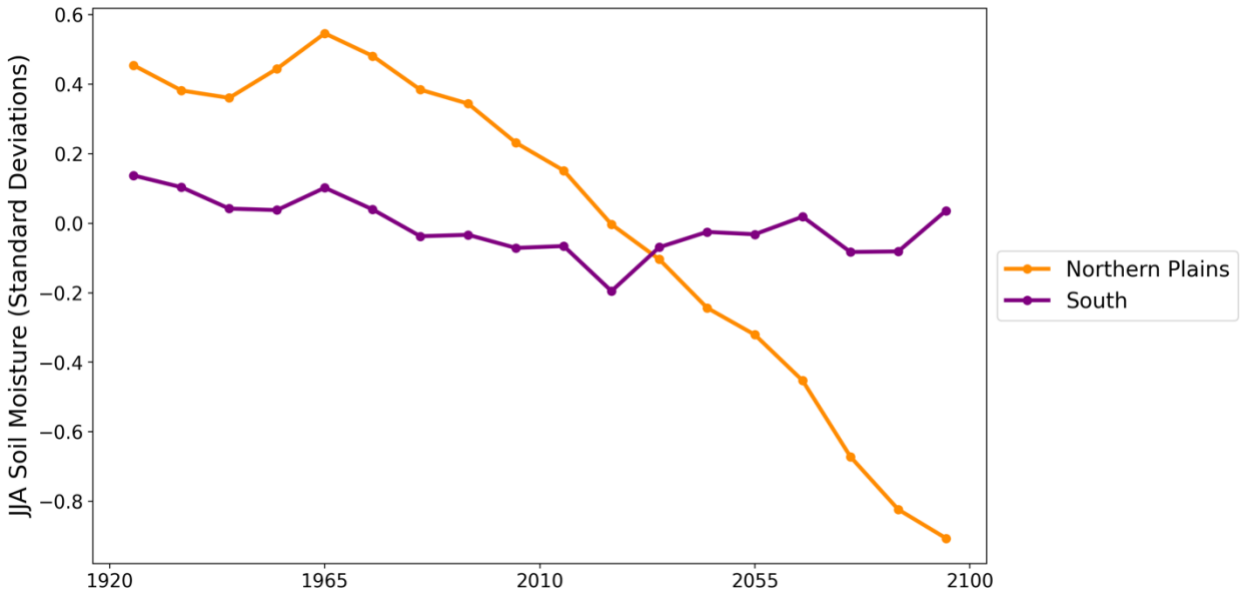

Figure 12. CESM1-LE soil moisture trends. By decade, average summer soil moisture in CESM1-LE for the South and Northern Plains regions. Soil moisture is measured in intra-summer fully-coupled preindustrial control simulation soil moisture standard deviations. The mean and seasonal cycle has been removed with respect to the period 1920-2100 for each ensemble member.

No visible trend is present in the South, as mean summer soil moisture appears to remain relatively constant throughout the simulations. However, in the Northern Plains, there is a clear decreasing trend. From the 1920s to the 2050s, mean soil moisture decreases by over half a

standard deviation. By the 2100s, the decrease has surpassed a full standard deviation. Regressing the residual component on one-week lagged soil moisture during Northern Plains heatwaves provides a coefficient of -0.29°C per standard deviation of soil moisture change. From the baseline of mean soil moisture in 1920-2010, this implies a potential amplification of the residual component of 0.19°C and 0.36°C for 2040-2049 and 2080-2089, respectively. These correspond to 27% and 51% increases in the residual component, which could increase the severity of heatwaves in this region.

4. Discussion and Conclusions

In this study we apply CCAs to daily summer temperature to estimate the contribution of concurrent atmospheric circulation to extreme heat events. As expected, we find that atmospheric circulation explains the majority of temperature anomalies during heatwaves. We then explore the "residual component", defined as the temperature anomaly unexplained by dynamical adjustment, which is largest in the central US. Here, 20%-30% of the heatwave temperature anomalies are not explained by the concurrent circulation, and soil moisture is identified as having an important role in amplifying temperatures beyond that expected from heatwave-associated circulation alone. Further, we present evidence that during events with the largest residual component (which should roughly align with the most extreme events) in the central US, negative soil moisture anomalies are present over a month in advance of the heatwave.

Before discussing the implications of these findings further, we note a number of caveats of our results. First, our analysis of a single model, CESM1, means that the results could reflect relationships that are not present in the true Earth system or other climate models; future work should establish consistency in other data sources. Second, we take advantage of long control

simulations that both improve the skill of our CCA method and remove the need to account for nonstationarity related to human influence on the climate system. Applying the same technique we use here to observational data would be more difficult and result in a noisier estimate of the circulation-induced component of temperature, owing to the much shorter data record and the presence of an anthropogenic forced response. This highlights the need for further statistical advances in dynamical adjustment that can improve the signal-to-noise ratio, such as those explored in e.g. Sippel et al. (2019). Third, CCAs assume a linear relationship between SLP and temperature, which is likely a simplification of the true relationship. As such, a portion of the residual component that we attributed to non-dynamical processes could instead reflect nonlinearities in the relationship between temperature and SLP. Fourth, insofar as SLP is affected by the land surface (such as the effect of surface temperature on thermal low development), it is possible that some of the dynamical component that we estimate may be better attributed to the land and not to the circulation. Replacing SLP with Z500 would not solve this issue of causality, as it too is affected by surface conditions. Finally, the CCA method has an inherent dependence on the domains chosen for both temperature and SLP. While our climate regions are sufficiently small that they are likely to experience heatwaves synchronously, and our SLP regions were chosen based on physical mechanisms, it is possible that results could differ with different regions. We are nevertheless encouraged by the similarity of our main results and those of Merrifield et al. (2017), who dynamically adjusted the US as a whole.

Despite these limitations, our methodology provides a general framework with which to parse the dynamical components of heatwaves from those resulting from other processes. The approach confirms the central US as a land-atmosphere coupling hot spot (e.g. Zhang et al. 2008; Merrifield et al. 2017; Vogel et al. 2017). In this region, we find that negative soil moisture

anomalies and positive dynamically-predicted temperature anomalies precede the hottest heatwaves by over a month (recall Figure 10). These anomalies suggest soil moisture as a source of heatwave predictability in the region and raise the possibility of positive feedbacks occurring between the land surface and the atmosphere as follows: The circulation patterns associated with positive dynamically-predicted temperatures would be expected to lead to negative soil moisture anomalies. In addition, it is possible that negative soil moisture anomalies, via reducing evapotranspiration and increasing sensible heating, could have an effect on circulation patterns that drives an increase in the dynamical component of temperature. Such a positive feedback has been identified in Europe, where Miralles et al. (2014) showed that during mega-heatwaves, soil desiccation enhanced temperatures by increasing entrainment of warm air into the boundary layer and Haarsma et al. (2009) demonstrated that warm easterly winds were driven by drier soils. In North America, Teng et al. (2019) found that prescribing low soil water in CESM1 during the summer led to positive geopotential height anomalies over North America and drove a circumglobal teleconnection response. While these studies support the idea of land-atmosphere feedbacks causing the persistent hot and dry conditions we observed, it is also plausible that circulation patterns consistent with positive temperature anomalies and drier soils are particularly persistent in the central US due to factors other than soil moisture feedbacks, such as remote ocean forcing.

While soil moisture provided a consistent explanation for the amplification of heatwaves in the central US, we did not find the same relationships for the remainder of the country. Circulation accounted for a larger proportion of temperature anomalies in the western and eastern US compared to the central US, but the dynamical prediction typically failed to explain 10%-20% of the anomalies. If the residuals resulted from unbiased methodological error, we

would expect that each event might have large positive or negative residuals, but on average they would be zero. The fact that the average dynamical component of temperature is always found to be less than the actual temperature anomaly indicates that there is a systematic underestimation. One explanation is that because we are filtering to particularly extreme events, the circulation patterns may be particularly distinct and possess fewer close analogs, leading to poorer prediction during these events. Given the large number of potential analogs in the CESM1 preindustrial simulation, this seems unlikely to fully explain the residual component. Other possibilities related to our CCA methodology are that SLP is an incomplete proxy for the atmospheric circulation, that the assumption of linearity between SLP and temperature does not hold for more extreme events, and/or that the time evolution of the circulation is relevant. Finally, there may be other variables beyond one-week lagged soil moisture that would help to explain the residual component in these regions.

Looking to the future, the CESM1-LE projects an increase in the probability of the heatwave- associated circulation patterns that we identified in the PiCTL in six out of nine regions, raising the possibility of a forced increase in heatwaves due to dynamical changes. However, from our analysis alone, the causality is unclear because some of the SLP patterns associated with heatwaves, such as thermal lows, could have been caused by the heatwaves themselves. Further, it is not guaranteed that the relationship between SLP and temperature is stationary. When dynamically adjusting the CESM1-LE using the PiCTL as SLP analogs (Deser et al. 2016) or dynamically adjusting observations, where history provides analogs, a trend in the distribution of SLP may make similar SLP events less analogous and reduce the utility of dynamical adjustment techniques.

Overall, this study demonstrated the application of CCAs to daily temperatures, which allows a focus on high-impact extreme heat events. We demonstrated a role for persistent soil moisture deficits and circulation anomalies in the most severe central US heatwaves, suggesting a role of land-atmosphere coupling and feedbacks. Having developed and tested our framework using a large climate model dataset, it would be useful to extend this analysis to observational data to confirm that the results hold. Finally, inasmuch as there is a strong link to the circulation, this technique could be applied to other extremes, such as high-precipitation events and droughts.

5. Supplementary Figures

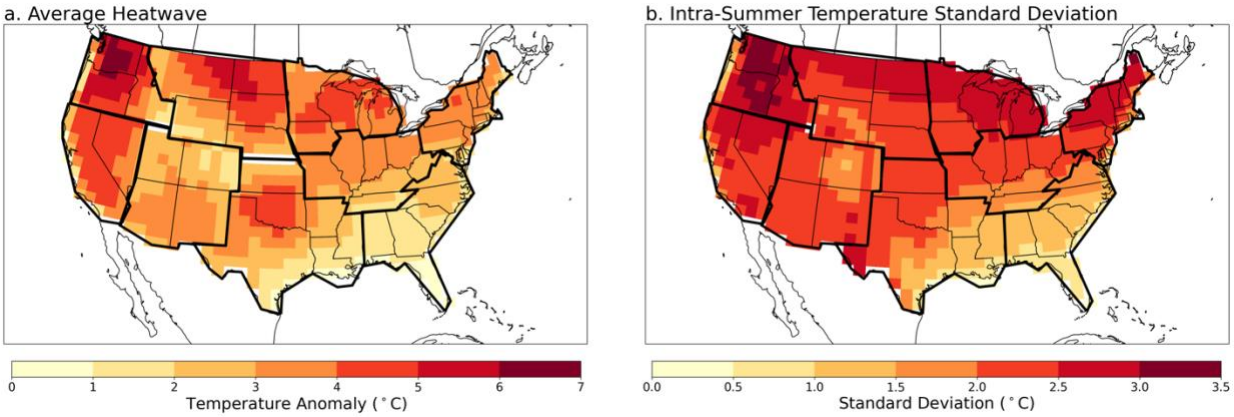

Figure S1. FixSST-PiCTL temperature anomalies and standard deviations. For the climatological mean sea surface temperature preindustrial control simulation, (a) Average temperature anomaly during heatwaves and (b) daily summer temperature standard deviation, calculated as the square root of the average of the variances calculated for each summer individually.

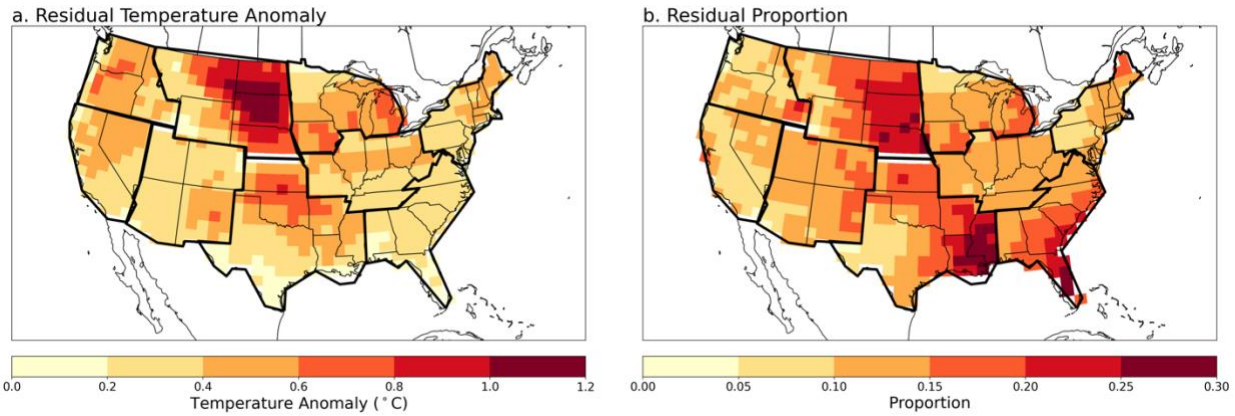

Figure S2. FixSST-PiCTL residual temperature anomaly and proportion. For heatwaves in the climatological mean sea surface temperature preindustrial control simulation, (a) average residual temperature anomaly during heatwaves after removing the average dynamical component from the temperature anomaly and (b) proportion of the average heatwave temperature anomaly accounted for by residual temperature anomaly.

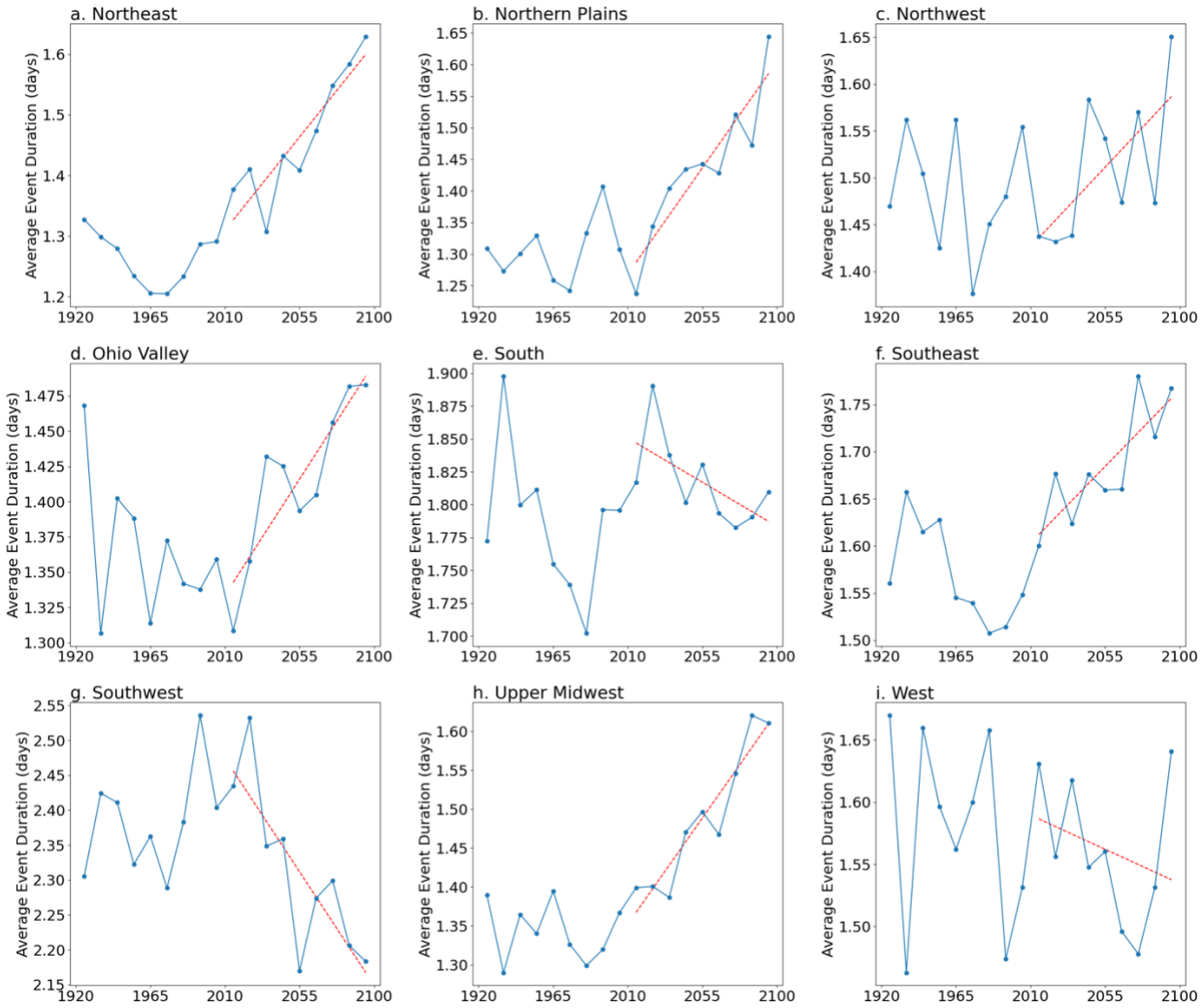

Figure S3. CESM1-LE SLP event duration trends. By decade, average length in days of separate, non-consecutive events with a correlation above 0.7 between daily summer sea level pressure patterns in CESM1-LE and the average sea level pressure pattern for fully-coupled preindustrial control simulation heatwaves. Linear trend lines for 2010-2099 are shown in red.

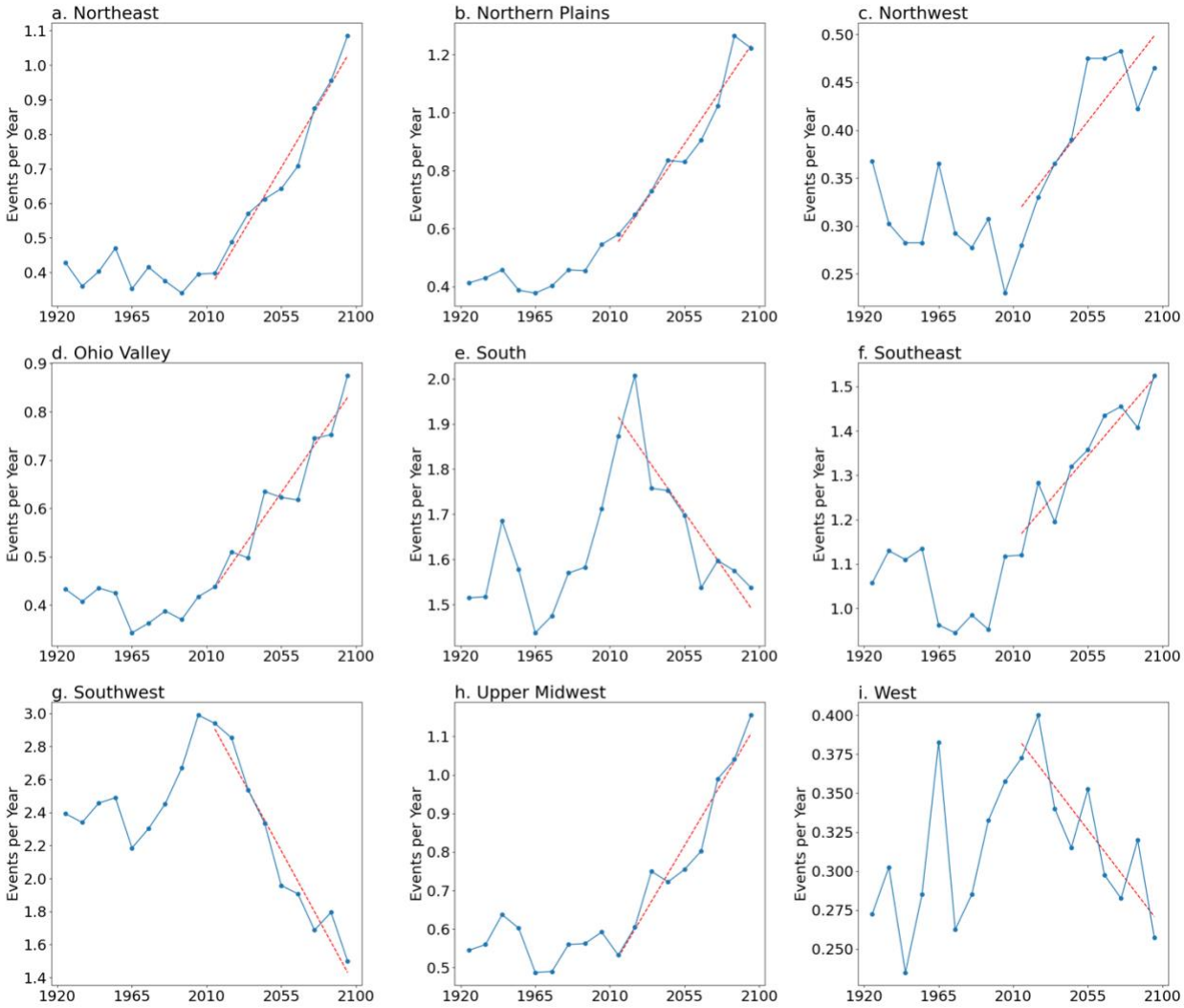

Figure S4. CESM1-LE SLP event count trends. By decade, average number of separate, non-consecutive events per year with a correlation above 0.7 between daily summer sea level pressure patterns in CESM1-LE and the average sea level pressure pattern for fully-coupled preindustrial control simulation heatwaves. Linear trend lines for 2010-2099 are shown in red.

6. References

Adams, R. E., C. C. Lee, E. T. Smith, and S. C. Sheridan, 2021: The relationship between atmospheric circulation patterns and extreme temperature events in north america. *Int. J. Climatol.*, **41 (1)**, 92–103, doi:10.1002/joc.6610.

Anderson, B. G., and M. L. Bell, 2009: Weather-related mortality: how heat, cold, and heat waves affect mortality in the united states. *Epidemiology*, **20 (2)**, 205–213, doi:10.1097/EDE.0b013e318190ee08.

Cook, B. I., T. R. Ault, and J. E. Smerdon, 2015: Unprecedented 21st century drought risk in the american southwest and central plains. *Science Advances*, **1 (1)**, doi:10.1126/sciadv.1400082.

Coumou, D., V. Petoukhov, S. Rahmstorf, S. Petri, and H. J. Schellnhuber, 2014: Quasi-resonant circulation regimes and hemispheric synchronization of extreme weather in boreal summer. *Proc. Natl. Acad. Sci. (USA)*, **111 (34)**, 12 331–12 336, doi:10.1073/pnas.1412797111.

Deser, C., L. Terray, and A. S. Phillips, 2016: Forced and internal components of winter air temperature trends over north america during the past 50 years: Mechanisms and implications. *J. Climate*, **29 (6)**, 2237 – 2258, doi:10.1175/JCLI-D-15-0304.1.

Fischer, E. M., S. I. Seneviratne, D. Lüthi, and C. Schär, 2007a: Contribution of land-atmosphere coupling to recent european summer heat waves. *Geophys. Res. Lett.*, **34 (6)**, doi:10.1029/2006GL029068.

Fischer, E. M., S. I. Seneviratne, P. L. Vidale, D. Lüthi, and C. Schär, 2007b: Soil moisture-atmosphere interactions during the 2003 european summer heat wave. *J. Climate*, **20 (20)**, 5081 – 5099, doi:10.1175/JCLI4288.1.

Gasparrini, A., and Coauthors, 2015: Mortality risk attributable to high and low ambient temperature: a multicountry observational study. *The Lancet*, **386 (9991)**, 369–375, doi:10.1016/S0140-6736(14)62114-0.

Gershunov, A., D. R. Cayan, and S. F. Iacobellis, 2009: The great 2006 heat wave over california and nevada: Signal of an increasing trend. *J. Climate*, **22 (23)**, 6181 – 6203, doi:10.1175/2009JCLI2465.1.

Goodman, J., M. Hurwitz, J. Park, and J. Smith, 2018: Heat and learning. Working Paper 24639, National Bureau of Economic Research. doi:10.3386/w24639.

Grotjahn, R., and Coauthors, 2016: North American extreme temperature events and related large scale meteorological patterns: a review of statistical methods, dynamics, modeling, and trends. *Climate Dyn.*, **46 (3)**, 1151–1184, doi:10.1007/s00382-015-2638-6.

Haarsma, R. J., F. Selten, B. v. Hurk, W. Hazeleger, and X. Wang, 2009: Drier mediterranean soils due to greenhouse warming bring easterly winds over summertime central europe. *Geophys. Res. Lett.*, **36 (4)**, doi:10.1029/2008GL036617.

Hauser, M., R. Orth, and S. I. Seneviratne, 2016: Role of soil moisture versus recent climate change for the 2010 heat wave in western russia. *Geophys. Res. Lett.*, **43 (6)**, 2819–2826, doi:10.1002/2016GL068036.

Heal, G., and J. Park, 2016: Temperature stress and the direct impact of climate change: A review of an emerging literature. *Review of Environmental Economics and Policy*, **10 (2)**, 1–17.

Hirschi, M., and Coauthors, 2011: Observational evidence for soil-moisture impact on hot extremes in southeastern Europe. *Nature Geoscience*, **4 (1)**, 17–21, doi:10.1038/ngeo1032.

Honda, Y., and Coauthors, 2014: Heat-related mortality risk model for climate change impact projection. *Environ Health Prev Med*, **19 (1)**, 56–63., doi:10.1007/s12199-013-0354-6.

Horton, R. M., J. S. Mankin, C. Lesk, E. Coffel, and C. Raymond, 2016: A Review of Recent Advances in Research on Extreme Heat Events. *Current Climate Change Reports*, **2 (4)**, 242–259, doi:10.1007/s40641-016-0042-x.

Hurrell, J. W., and Coauthors, 2013: The community earth system model: A framework for collabo- rative research. *Bull. Amer. Meteor. Soc.*, **94 (9)**, 1339 – 1360, doi:10.1175/BAMS-D-12-00121. 1.

Jaeger, E. B., and S. I. Seneviratne, 2011: Impact of soil moisture–atmosphere coupling on European climate extremes and trends in a regional climate model. *Climate Dyn.*, **36 (9)**, 1919–1939, doi:10.1007/s00382-010-0780-8.

Karl, T., and W. J. Koss, 1984: Historical climatology series ; 4-3. Regional and national monthly, seasonal, and annual temperature weighted by area, 1895-1983. URL https://repository.library. noaa.gov/view/noaa/10238.

Kay, J. E., and Coauthors, 2015: The community earth system model (cesm) large ensemble project: A community resource for studying climate change in the presence of internal climate variability. *Bull. Amer. Meteor. Soc.*, **96 (8)**, 1333 – 1349, doi:10.1175/BAMS-D-13-00255.1.

Kjellstrom, T., R. Kovats, S. Lloyd, T. Holt, and R. Tol, 2009: The direct impact of climate change on regional labor productivity. *Arch Environ Occup Health*, **64 (4)**, 217–227, doi: 10.1080/19338240903352776.

Kornhuber, K., D. Coumou, E. Vogel, C. Lesk, J. F. Donges, J. Lehmann, and R. M. Horton, 2020: Amplified Rossby waves enhance risk of concurrent heatwaves in major breadbasket regions. *Nature Climate Change*, **10 (1)**, 48–53, doi:10.1038/s41558-019-0637-z.

Kornhuber, K., S. Osprey, D. Coumou, S. Petri, V. Petoukhov, S. Rahmstorf, and L. Gray, 2019: Extreme weather events in early summer 2018 connected by a recurrent hemispheric wave-7 pattern. *Environmental Research Letters*, **14 (5)**, 054 002, doi:10.1088/1748-9326/ab13bf.

Koster, R. D., and M. J. Suarez, 2001: Soil moisture memory in climate models. *Journal of Hydrometeorology*, **2 (6)**, 558 – 570, doi:10.1175/1525-7541(2001)002<0558:SMMICM>2.0.CO;2.

Lau, N.-C., and M. J. Nath, 2012: A model study of heat waves over north america: Meteorological aspects and projections for the twenty-first century. *J. Climate*, **25 (14)**, 4761 – 4784, doi: 10.1175/JCLI-D-11-00575.1.

Lehner, F., C. Deser, I. R. Simpson, and L. Terray, 2018: Attributing the u.s. southwest's recent shift into drier conditions. *Geophys. Res. Lett.*, **45 (12)**, 6251–6261, doi:10.1029/2018GL078312.

Lehner, F., C. Deser, and L. Terray, 2017: Toward a new estimate of "time of emergence" of anthropogenic warming: Insights from dynamical adjustment and a large initial-condition model ensemble. *J. Climate*, **30 (19)**, 7739 – 7756, doi:10.1175/JCLI-D-16-0792.1.

Lo, M.-H., T.-H. Kuo, H.-W. Wey, C.-W. Lan, and J.-P. Chen, 2017: *Land Processes as the Forcing of Extremes*, chap. 5, 75–92. American Geophysical Union (AGU), doi:10.1002/9781119068020. ch5.

Loikith, P. C., and A. J. Broccoli, 2012: Characteristics of observed atmospheric circulation patterns associated with temperature extremes over north america. *J. Climate*, **25 (20)**, 7266 – 7281, doi:10.1175/JCLI-D-11-00709.1.

Lorenz, R., E. B. Jaeger, and S. I. Seneviratne, 2010: Persistence of heat waves and its link to soil moisture memory. *Geophys. Res. Lett.*, **37 (9)**, doi:10.1029/2010GL042764.

Mankin, J. S., J. E. Smerdon, B. I. Cook, A. P. Williams, and R. Seager, 2017: The curious case of projected twenty-first-century drying but greening in the american west. *J. Climate*, **30 (21)**, 8689 – 8710, doi:10.1175/JCLI-D-17-0213.1.

McKinnon, K. A., A. Rhines, M. P. Tingley, and P. Huybers, 2016: Long-lead predictions of eastern United States hot days from Pacific sea surface temperatures. *Nature Geoscience*, **9 (5)**, 389–394, doi:10.1038/ngeo2687.

Meehl, G. A., and C. Tebaldi, 2004: More intense, more frequent, and longer lasting heat waves in the 21st century. *Science*, **305 (5686)**, 994–997, doi:10.1126/science.1098704.

Merrifield, A., F. Lehner, S.-P. Xie, and C. Deser, 2017: Removing circulation effects to assess central u.s. land-atmosphere interactions in the cesm large ensemble. *Geophys. Res. Lett.*, **44 (19)**, 9938–9946, doi:10.1002/2017GL074831.

Merrifield, A. L., I. R. Simpson, K. A. McKinnon, S. Sippel, S.-P. Xie, and C. Deser, 2019: Local and nonlocal land surface influence in european heatwave initial condition ensembles. *Geophysical Research Letters*, **46 (23)**, 14 082–14 092, doi:10.1029/2019GL083945.

Miralles, D. G., P. Gentine, S. I. Seneviratne, and A. J. Teuling, 2019: Land–atmospheric feedbacks during droughts and heatwaves: state of the science and current challenges. *Annals of the New York Academy of Sciences*, **1436 (1)**, 19–35, doi:10.1111/nyas.13912.

Miralles, D. G., A. J. Teuling, C. C. van Heerwaarden, and J. V.-G. de Arellano, 2014: Mega-heatwave temperatures due to combined soil desiccation and atmospheric heat accumulation. *Nature Geoscience*, **7 (5)**, 345–349, doi:10.1038/ngeo2141.

Mueller, B., and S. I. Seneviratne, 2012: Hot days induced by precipitation deficits at the global scale. *Proc. Natl. Acad. Sci. (USA)*, **109 (31)**, 12 398–12 403, doi:10.1073/pnas.1204330109.

Pfahl, S., and H. Wernli, 2012: Quantifying the relevance of atmospheric blocking for co-located temperature extremes in the northern hemisphere on (sub-)daily time scales. *Geophys. Res. Lett.*, **39 (12)**, doi:10.1029/2012GL052261.

Romero-Lankao, P., J. Smith, D. Davidson, N. Diffenbaugh, P. Kinney, P. Kirshen, P. Kovacs, and L. V. Ruiz, 2014: North america. *Climate Change 2014: Impacts, Adaptation, and Vulnerability. Part B: Regional Aspects. Contribution of Working Group II to the Fifth Assessment Report of the Intergovernmental Panel on Climate Change*, Cambridge University Press, 1439–1498.

Röthlisberger, M., L. Frossard, L. F. Bosart, D. Keyser, and O. Martius, 2019: Recurrent synoptic- scale rossby wave patterns and their effect on the persistence of cold and hot spells. *J. Climate*, **32 (11)**, 3207 – 3226, doi:10.1175/JCLI-D-18-0664.1.

Schlenker, W., and M. J. Roberts, 2009: Nonlinear temperature effects indicate severe damages to u.s. crop yields under climate change. *Proc. Natl. Acad. Sci. (USA)*, **106 (37)**, 15 594–15 598, doi:10.1073/pnas.0906865106.

Schubert, S., H. Wang, and M. Suarez, 2011: Warm season subseasonal variability and climate extremes in the northern hemisphere: The role of stationary rossby waves. *J. Climate*, **24 (18)**, 4773 – 4792, doi:10.1175/JCLI-D-10-05035.1.

Screen, J. A., and I. Simmonds, 2014: Amplified mid-latitude planetary waves favour particular regional weather extremes. *Nature Climate Change*, **4 (8)**, 704–709, doi:10.1038/nclimate2271.

Seager, R., M. Ting, C. Li, N. Naik, B. Cook, J. Nakamura, and H. Liu, 2013: Projections of declining surface-water availability for the southwestern United States. *Nature Climate Change*, **3 (5)**, 482–486, doi:10.1038/nclimate1787.

Selten, F. M., R. Bintanja, R. Vautard, and B. J. J. M. van den Hurk, 2020: Future continental summer warming constrained by the present-day seasonal cycle of surface hydrology. *Scientific Reports*, **10 (1)**, 4721, doi:10.1038/s41598-020-61721-9.

Seneviratne, S. I., T. Corti, E. L. Davin, M. Hirschi, E. B. Jaeger, I. Lehner, B. Orlowsky, and A. J. Teuling, 2010: Investigating soil moisture–climate interactions in a changing climate: A review. *Earth-Science Reviews*, **99 (3)**, 125–161, doi:10.1016/j.earscirev.2010.02.004.

Seneviratne, S. I., and Coauthors, 2006: Soil moisture memory in agcm simulations: Analysis of global land-atmosphere coupling experiment (glace) data. *Journal of Hydrometeorology*, **7 (5)**, 1090 – 1112, doi:10.1175/JHM533.1.

Seneviratne, S. I., and Coauthors, 2013: Impact of soil moisture-climate feedbacks on cmip5 projections: First results from the glace-cmip5 experiment. *Geophys. Res. Lett.*, **40 (19)**, 5212–5217, doi:10.1002/grl.50956.

Sippel, S., N. Meinshausen, A. Merrifield, F. Lehner, A. G. Pendergrass, E. Fischer, and R. Knutti, 2019: Uncovering the forced climate response from a single ensemble member using statistical learning. *J. Climate*, **32 (17)**, 5677 – 5699, doi:10.1175/JCLI-D-18-0882.1.

Song, X., S. Wang, Y. Hu, M. Yue, T. Zhang, Y. Liu, J. Tian, and K. Shang, 2017: Impact of ambient temperature on morbidity and mortality: An overview of reviews. *Science of The Total Environment*, **586**, 241–254, doi:10.1016/j.scitotenv.2017.01.212.

Stéfanon, M., P. Drobinski, F. D'Andrea, C. Lebeaupin-Brossier, and S. Bastin, 2014: Soil moisture- temperature feedbacks at meso-scale during summer heat waves over Western Europe. *Climate Dyn.*, **42 (5)**, 1309–1324, doi:10.1007/s00382-013-1794-9.

Sánchez, B., A. Rasmussen, and J. R. Porter, 2014: Temperatures and the growth and development of maize and rice: a review. *Global Change Biology*, **20 (2)**, 408–417, doi:10.1111/gcb.12389.

Taylor, K. E., R. J. Stouffer, and G. A. Meehl, 2012: An overview of cmip5 and the experiment design. *Bull. Amer. Meteor. Soc.*, **93 (4)**, 485 – 498, doi:10.1175/BAMS-D-11-00094.1.

Teng, H., G. Branstator, A. B. Tawfik, and P. Callaghan, 2019: Circumglobal response to prescribed soil moisture over north america. *J. Climate*, **32 (14)**, 4525 – 4545, doi:10.1175/JCLI-D-18-0823. 1.

Teng, H., G. Branstator, H. Wang, G. A. Meehl, and W. M. Washington, 2013: Probability of US heat waves affected by a subseasonal planetary wave pattern. *Nature Geoscience*, **6 (12)**, 1056–1061, doi:10.1038/ngeo1988.

Teuling, A. J., and Coauthors, 2009: A regional perspective on trends in continental evaporation. *Geophys. Res. Lett.*, **36 (2)**, doi:10.1029/2008GL036584.

Thomas, N. P., M. G. Bosilovich, A. B. M. Collow, R. D. Koster, S. D. Schubert, A. Dezfuli, and S. P. Mahanama, 2020: Mechanisms associated with daytime and nighttime heat waves over the contiguous united states. *J. Appl. Meteor. Climatol.*, **59 (11)**, 1865 – 1882, doi:10.1175/ JAMC-D-20-0053.1.

Vargas-Zeppetello, L. R., E. Tétreault-Pinard, D. S. Battisti, and M. B. Baker, 2020: Identifying the sources of continental summertime temperature variance using a diagnostic model of land-atmosphere interactions. *J. Climate*, **33 (9)**, 3547 – 3564, doi:10.1175/JCLI-D-19-0276.1.

Vogel, E., M. G. Donat, L. V. Alexander, M. Meinshausen, D. K. Ray, D. Karoly, N. Meinshausen, and K. Frieler, 2019: The effects of climate extremes on global agricultural yields. *Environmental Research Letters*, **14 (5)**, 054 010, doi:10.1088/1748-9326/ab154b.

Vogel, M. M., R. Orth, F. Cheruy, S. Hagemann, R. Lorenz, B. J. J. M. van den Hurk, and S. I. Seneviratne, 2017: Regional amplification of projected changes in extreme temperatures strongly

controlled by soil moisture-temperature feedbacks. *Geophys. Res. Lett.*, **44 (3)**, 1511– 1519, doi:10.1002/2016GL071235.

Vose, R., D. Easterling, K. Kunkel, A. LeGrande, and M. Wehner, 2017: Temperature changes in the united states. *Climate Science Special Report: Fourth National Climate Assessment, Volume I*, U.S. Global Change Research Program, 185–206, doi:10.7930/J0N29V45.

Wehrli, K., B. P. Guillod, M. Hauser, M. Leclair, and S. I. Seneviratne, 2019: Identifying key driving processes of major recent heat waves. *Journal of Geophysical Research: Atmospheres*, **124 (22)**, 11 746–11 765, doi:10.1029/2019JD030635.

Wilks, D. S., 2016: "The stippling shows statistically significant grid points": How research results are routinely overstated and overinterpreted, and what to do about it. *Bull. Amer. Meteor. Soc.*, **97 (12)**, 2263 – 2273, doi:10.1175/BAMS-D-15-00267.1.

Yang, Z., F. Dominguez, and X. Zeng, 2019: Large and local-scale features associated with heat waves in the United States in reanalysis products and the NARCCAP model ensemble. *Climate Dyn.*, **52 (3)**, 1883–1901, doi:10.1007/s00382-018-4414-x.

Ye, X., R. Wolff, W. Yu, P. Vaneckova, X. Pan, and S. Tong, 2012: Ambient temperature and morbidity: A review of epidemiological evidence. *Environmental Health Perspectives*, **120 (1)**, 19–28, doi:10.1289/ehp.1003198.

Zhang, J., W.-C. Wang, and L. R. Leung, 2008: Contribution of land-atmosphere coupling to summer climate variability over the contiguous united states. *Journal of Geophysical Research: Atmospheres*, **113 (D22)**, doi:10.1029/2008JD010136.